

# Dynamical Model of $J/\Psi$ photo-production on the nucleon

S. Sakinah,<sup>1,\*</sup> T.-S. H. Lee,<sup>2,†</sup> and H. M. Choi<sup>1,‡</sup>

<sup>1</sup>*Department of Physics, Kyungpook National University, Daegu 41566, South Korea*

<sup>2</sup>*Physics Division, Argonne National Laboratory, Argonne, Illinois 60439, USA*

(Dated: March 5, 2024)

A dynamical model based on a phenomenological charm quark-nucleon ( $c$ -N) potential  $v_{cN}$  and the Pomeron-exchange mechanism is constructed to investigate the  $J/\Psi$  photo-production on the nucleon from threshold to invariant mass  $W = 300$  GeV. The  $J/\Psi$ -N potential,  $V_{J/\Psi N}(r)$ , is constructed by folding  $v_{cN}$  into the wavefunction  $\Phi_{J/\Psi}(c\bar{c})$  of  $J/\Psi$  within a Constituent Quark Model (CQM) of Ref. [43]. A photo-production amplitude is also generated by  $v_{cN}$  by a  $c\bar{c}$ -loop integration over the  $\gamma \rightarrow c\bar{c}$  vertex function and  $\Phi_{J/\Psi}(c\bar{c})$ . No commonly used Vector Meson Dominance assumption is used to define this photo-production amplitude which is needed to describe the data near the threshold. The  $c$ -N potential  $v_{cN}(r)$  is parameterized in a form such that the predicted  $V_{J/\Psi N}(r)$  at large distances has the same Yukawa potential form extracted from a Lattice QCD (LQCD) calculation of Ref. [18]. The parameters of  $v_{cN}$  are determined by fitting the total cross section data of JLab by performing calculations that include  $J/\Psi$ -N final state interactions (FSI). The resulting differential cross sections  $d\sigma/dt$  are found in good agreements with the data. It is shown that the FSI effects dominate the cross section in the very near-threshold region, allowing for sensitive testing of the predicted  $J/\Psi$ -N scattering amplitudes. By imposing the constraints of  $J/\Psi$ -N potential extracted from the LQCD calculation of Ref. [18], we have obtained three  $J/\Psi$ -N potentials which fit the JLab data equally well. The resulting  $J/\Psi$ -N scattering lengths are in the range of  $a = (-0.05 \text{ fm} \sim -0.25 \text{ fm})$ . With the determined  $v_{cN}(r)$  and the wavefunctions generated from the same CQM, the constructed model is used to predict the cross sections of photo-production of  $\eta_c(1S)$  and  $\Psi(2S)$  mesons for future experimental tests.

## I. INTRODUCTION

It is well recognized [1] that the information on the interactions between the  $J/\Psi$  meson and the nucleon(N) can improve our understanding of the roles of gluons ( $g$ ) in determining the structure of hadrons and hadron-hadron interactions. In addition, a model of the  $J/\Psi$ -N interaction is needed to understand the nucleon resonances  $N^*(P_c)$  reported by the LHCb collaboration [2–5]. It is also needed to extract the gluonic distributions in nuclei, and to study the existence of nuclei with hidden charms [6–10].

The leading  $J/\Psi$ -N interaction is the two-gluon exchange mechanism, as illustrated in Fig. 1. Higher order multi-gluon exchange effects can not be neglected in the non-perturbative region. By using continuum and lattice

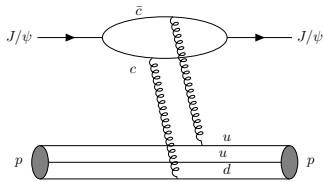


FIG. 1: Two gluon exchange mechanism of  $J/\psi$ -N reaction in QCD.

studies at low energies and the heavy quark effective field theory and perturbative QCD (PQCD) at high energies, the  $J/\Psi$ -N interaction can be estimated.

Several attempts had been made to determine the  $J/\Psi$ -N interactions. Peskin [11] applied the operator product expansion to evaluate the strength of the color field emitted by heavy  $q\bar{q}$  systems, and suggested [12] that the van der Waals force induced by the color field of  $J/\Psi$  on nucleons can generate an attractive short-range  $J/\Psi$ -N interaction. The results of Peskin were used by Luke, Manohar, and Savage [13] to predict, using the effective field theory method, the  $J/\Psi$ -N forward scattering amplitude which was then used to get an estimation that  $J/\Psi$  can have a few MeV/nucleon attraction in nuclear matter. The  $J/\Psi$ -N forward scattering amplitude of Ref. [13] was further investigated by Brodsky and Miller [14] to derive a  $J/\Psi$ -N potential which gives a  $J/\Psi$ -N scattering length of  $-0.24$  fm. The result of Peskin was also used by Kaidalov and Volkovitsky [15], who differed from Ref. [14] in evaluating the gluon content in the nucleon, to give a much smaller scattering length of  $-0.05$  fm. In LQCD calculations using the approach of Refs. [16, 17], Kawanai and Sasaki [18, 19] obtained an attractive  $J/\Psi$ -N potential of the Yukawa form  $V_{J/\Psi N, J/\Psi N} = -\alpha e^{-\mu r}/r$  with  $\alpha = 0.1$  and  $\mu = 0.6$  GeV, which gives a scattering length of  $-0.09$  fm.

To make progress, it is necessary to have experimental information on the  $J/\Psi$ -N scattering to test the theoretical results described above and future LQCD calculations. One can adopt the traditional approach for determining the vector meson-nucleon (V-N) interaction the Vector Meson Dominance (VMD) assump-

\* ssakinahf@knu.ac.kr

† tshlee@anl.gov

‡ homyoung@knu.ac.kr

tion to extract  $J/\Psi$ -N cross sections from the data of  $J/\Psi$  photo-production reactions. In this approach, the incoming photon is converted into a vector meson  $V$  which is then scattered from the nucleon, as illustrated in Fig. 2. However the approach based on VMD is not valid for  $J/\Psi$  because the VMD coupling constant is determined by the  $J/\Psi \rightarrow \gamma \rightarrow e^+e^-$  decay width at  $q^2 = m_{J/\Psi}^2 \sim 9 \text{ GeV}^2$  which is far from  $q^2 = 0$  of the  $\gamma + p \rightarrow J/\Psi + p$  reaction. Furthermore, the use of VMD for  $J/\Psi$  is questionable as discussed in Ref. [20]. In addition, the  $J/\Psi + N \rightarrow J/\Psi + N$  transition amplitude  $t_{J/\Psi N, J/\Psi N}(k, q, W)$  near threshold is far off-shell; for example, at  $W = (m_N + m_{J/\Psi}) + 0.5 \text{ GeV}$ , the incoming  $\gamma N$  relative momentum is  $q = 0.8 \text{ GeV}$  which is much larger than the outgoing  $J/\Psi$ -N relative momentum  $k = 0.1 \text{ GeV}$  in the center of mass (CM) system. Thus the VMD approach is clearly not directly applicable for describing  $J/\Psi + N \rightarrow J/\Psi + N$  in the near threshold energy region.

In this paper, we present a reaction model for extracting the  $J/\Psi$  scattering amplitudes from the data of  $\gamma + N \rightarrow J/\Psi + N$  reactions of Jefferson Laboratory (JLab) [21, 22]. In the meantime, we will obtain phenomenological  $J/\Psi$ -N potentials,  $V_{J/\Psi N, J/\Psi N}$ , for investigating nuclear reactions involving  $J/\Psi$  meson. No VMD is assumed by taking the  $c\bar{c}$  structure of  $J/\Psi$  into account to define the model Hamiltonian. For simplicity in this exploring work, we will follow the Pomeron-exchange model of Donnachie and Landshoff (DL) [23] to neglect the quark sub-structure of the nucleon and assume that that the interactions between the charm-anticharm ( $c\bar{c}$ ) quarks in  $J/\Psi$  and the nucleon can be defined by a phenomenological quark-N potential  $v_{cN}$ . It follows that the  $\gamma + N \rightarrow J/\Psi + N$  transition amplitude,  $B_{\gamma N, J/\Psi N}$ , and the  $J/\Psi + N \rightarrow J/\Psi + N$  potential,  $V_{J/\Psi N}$ , are defined by  $c\bar{c}$ -loop mechanisms, as illustrated in Fig. 3. Following the dynamical formulation [24–27] within which the unitarity condition requires that  $J/\Psi$ -N final state interaction (FSI) effects must be included and the total amplitude of  $\gamma + N \rightarrow J/\psi + N$  is of the form

$$T_{\gamma N, J/\Psi N}^D = B_{\gamma N, J/\Psi N} + T_{\gamma N, J/\Psi N}^{(fsi)}, \quad (1)$$

with

$$T_{\gamma N, J/\Psi N}^{(fsi)} = B_{\gamma N, J/\Psi N}(W) G_{J/\Psi N} T_{J/\Psi N, J/\Psi N}, \quad (2)$$

where  $G_{J/\Psi N}$  is the  $J/\Psi$ -N propagator, and  $T_{J/\Psi N, J/\Psi N}$  is the  $J/\Psi$ -N scattering amplitude calculated from the

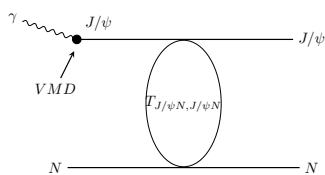


FIG. 2:  $J/\Psi$ -N interaction within the VMD assumption.

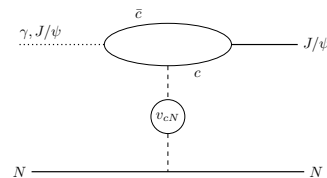


FIG. 3: Quark-antiquark loop mechanism within assuming the  $v_{cN}$  as quark interaction in  $J/\Psi$ -N reaction.

$J/\Psi$ -N potential,  $V_{J/\Psi N}(r)$ , by solving the following Lippman-Schwinger Equation

$$T_{J/\Psi N, J/\Psi N} = V_{J/\Psi N, J/\Psi N} + V_{J/\Psi N, J/\Psi N} G_{J/\Psi N} T_{J/\Psi N, J/\Psi N}. \quad (3)$$

To also describe data up to 300 GeV [21, 22, 28, 29], we add the Pomeron-exchange amplitude  $T_{\gamma N, J/\Psi N}^{\text{Pom}}$  of DL, reviewed in Ref. [1], such that the total amplitude can be used to investigate nuclear reactions involving  $J/\Psi$  at all energies. To be consistent, the Pomeron-exchange amplitude should also be defined by the similar  $c\bar{c}$ -loop mechanism of Fig. 3. By using a hadron model [30, 31] based on Dyson-Schwinger equation (DSE) of QCD, such a quark-loop Pomeron-exchange model was explored in Refs. [32, 33]. It will be interesting to use the recent DSE models [35–42] to improve the results of Refs. [32, 33]. Within the Hamiltonian formulation of this work, it requires a realistic Constituent Quark Model (CQM) to generate the  $J/\Psi$  wavefunction and careful treatments of relativistic kinematic effects within Dirac’s formulation of relativistic Quantum Mechanics [34]. We therefore will not pursue this here. Rather we focus on the near the threshold region, and any effects from Pomeron-exchange which is very weak in the near threshold region, can be considered as an estimate of uncertainties of the results presented in this paper.

Since the Pomeron-exchange amplitude  $T_{\gamma N, J/\Psi N}^{\text{Pom}}$  has been determined in Ref. [1], our task is to develop a model for calculating the amplitude  $T_{\gamma N, J/\Psi N}^D$  defined by Eqs. (1)-(3). As defined by the loop-mechanism, Fig. 3, the  $J/\Psi$ -N potential,  $V_{J/\Psi N}(r)$ , is constructed by folding  $v_{cN}(r)$  into the wavefunction  $\Phi_{J/\Psi}$ . By using the  $\Phi_{J/\Psi}$  from the CQM of Ref. [43], the amplitude  $T_{\gamma N, J/\Psi N}^D$  is completely determined by the  $c$ -N potential  $v_{cN}(r)$ . To establish correspondence with the LQCD calculations, the parametrization is chosen such that the predicted  $V_{J/\Psi N}(r)$  at large distances exhibits the same Yukawa potential form extracted from a LQCD calculation of [18].

We determine the parameters of  $v_{cN}$  by fitting the total cross section data of JLab’s Hall-D [21]. As will be presented later, the resulting differential cross sections  $d\sigma/dt$  are in reasonably good agreements with the data from JLab’s Hall-C [22]. More importantly, it is shown that the FSI effects dominate the cross section in the

very near-threshold region, allowing for sensitive testing of the predicted  $J/\Psi$ -N scattering amplitudes. Within the experimental uncertainties, this procedure allow us to obtain four  $J/\Psi$ -N potentials which all fit the available JLab data reasonably well. They however predict rather different cross sections near threshold and the resulting  $J/\Psi$ -N scattering lengths. More extensive and precise data in the very near threshold region are needed for making further progress.

By using the determined  $c$ -N potential  $v_{cN}(r)$  and the wavefunctions generated from the same CQM of Ref. [43], we can apply the constructed dynamical model to predict the cross sections of photo-production of the other Charmonium states. The results for the production of  $\eta_c(1S)$  and  $\Psi(2S)$  mesons are presented for future experimental tests at JLab and the future Electron-ion colliders (EIC).

Here we note that the JLab data of  $J/\Psi$  photo-production had also been investigated by using models based on two- and three-gluons exchange mechanisms [44], Generalized Parton Distribution (GPD) of the nucleon [45], and the Holographic QCD [46]. All of these approaches have rather different assumptions in treating the quark sub-structure of  $J/\Psi$ . They are distinctively different from our approach which accounts for the  $c\bar{c}$ -loop mechanisms in calculating both the  $J/\Psi$  photo-production amplitudes and  $J/\Psi$ -N final-state interactions. Thus their objective is not to extract  $J/\Psi$ -N interactions at low energies, as we are trying to achieve in this work.

In section II, we present our formulation. The results are presented in section III. Section IV is for giving a summary and discussing the possible future improvements.

## II. FORMULATION

We follow Ref. [47] to use the normalization  $\langle \mathbf{k}|\mathbf{k}' \rangle = \delta(\mathbf{k} - \mathbf{k}')$  for plane wave state  $|\mathbf{k}\rangle$  and  $\langle \phi_\alpha|\phi_\beta \rangle = \delta_{\alpha,\beta}$  for bound state  $|\phi_\alpha\rangle$ . The  $J/\Psi$  meson will be denoted as  $V$  in the rest of the paper.

The differential cross section of vector meson photo-production reaction,  $\gamma(\mathbf{q}, \lambda_\gamma) + N(\mathbf{p}, m_s) \rightarrow V(\mathbf{k}, \lambda_V) + N(\mathbf{p}', m'_s)$ , is calculated from [1]

$$\frac{d\sigma_{VN,\gamma N}}{d\Omega} = \frac{(2\pi)^4}{|\mathbf{q}|^2} \frac{|\mathbf{k}| E_V(\mathbf{k}) E_N(\mathbf{p})}{W} \frac{|\mathbf{q}|^2 E_N(\mathbf{q})}{W} \times \frac{1}{4} \sum_{\lambda_V, m'_s} \sum_{\lambda_\gamma, m_s} |\langle \mathbf{k}, \lambda_V m'_s | T_{VN,\gamma N} | \mathbf{q}, \lambda_\gamma m_s \rangle|^2, \quad (4)$$

where  $m_s^{(\prime)}$  denotes the  $z$ -component of the initial (final) state nucleon spin, and  $\lambda_V$  and  $\lambda_\gamma$  are the helicities of vector meson  $V$  and photon  $\gamma$ , respectively. In the CM frame, the magnitudes of  $|\mathbf{p}| = -|\mathbf{q}| = -q$  and  $|\mathbf{p}'| = -|\mathbf{k}| = -k$  are defined by the invariant mass  $W = q + E_N(q) = E_V(\mathbf{k}) + E_N(\mathbf{p}')$ .

The reaction amplitude  $T_{VN,\gamma N} = T_{VN,\gamma N}(W)$  can be decomposed into the sum of the dynamical scattering am-

plitude  $T^D$  and the Pomeron-exchange amplitude  $T^{\text{Pom}}$  as [1]

$$T_{VN,\gamma N} = T_{VN,\gamma N}^D + T_{VN,\gamma N}^{\text{Pom}}. \quad (5)$$

We shall describe each amplitude in the following subsections.

### A. Dynamical model for $T^D$

Following the dynamical approach of Refs. [24–27], the amplitude  $T^D$  is calculated from using the following Hamiltonian

$$H = H_0 + \Gamma_{\gamma,c\bar{c}} + v_{c\bar{c}} + v_{cN}, \quad (6)$$

where  $H_0$  is the free Hamiltonian,  $v_{cN}$  is a phenomenological quark-nucleon potential to be determined,  $v_{c\bar{c}}$  is the  $c\bar{c}$  potential of CQM, and  $\Gamma_{\gamma,c\bar{c}}$  is the electromagnetic coupling of  $\gamma \rightarrow c\bar{c}$  defined by

$$\langle \mathbf{q} | \Gamma_{\gamma,c\bar{c}} | \mathbf{k}_1, \mathbf{k}_2 \rangle = \frac{1}{\sqrt{2|\mathbf{q}|}} \frac{1}{\sqrt{2E_c(\mathbf{k}_1)}} \frac{1}{\sqrt{2E_c(\mathbf{k}_2)}} \times \frac{e_c}{(2\pi)^{3/2}} [\bar{u}(\mathbf{k}_1) \gamma^\mu \epsilon_\mu(q) v(\mathbf{k}_2)]. \quad (7)$$

Here  $e_c$  is the charge of the charmed quark,  $\epsilon_\mu(q)$  is the photon polarization vector,  $\bar{u}(\mathbf{k}_1)$  and  $v(\mathbf{k}_2)$  are the Dirac spinors with the normalization  $\bar{u}(\mathbf{k})u(\mathbf{k}) = \bar{v}(\mathbf{k})v(\mathbf{k}) = 1$ .

Using the potential  $v_{c\bar{c}}(r)$  in the Hamiltonian, the wavefunction  $|\phi_V\rangle$  of the  $J/\Psi$  is obtained by solving the bound-state equation within a CQM developed by Segovia et al. [43], expressed as:

$$(H_0 + v_{c\bar{c}}) |\phi_V\rangle = E_V |\phi_V\rangle. \quad (8)$$

Here, we assume a simple  $s$ -wave wavefunction  $\phi_{\mathbf{p}_V}(\mathbf{k}, \mathbf{k}') \equiv \langle \phi_{V,\mathbf{p}_V}^{J_V m_V} | \mathbf{k} m_{s_c}, \mathbf{k}' m'_{s_{\bar{c}}} \rangle$  and have the following matrix elements

$$\phi_{\mathbf{p}_V}(\mathbf{k}, \mathbf{k}') = \delta(\mathbf{p}_V - \mathbf{k} - \mathbf{k}') \langle J_V m_V | \frac{1}{2} \frac{1}{2} m_{s_c} m'_{s_{\bar{c}}} \rangle \phi(\bar{\mathbf{k}}), \quad (9)$$

where  $\mathbf{p}_V$  is the momentum of  $J/\Psi$ ,  $\mathbf{k}^{(\prime)}$  is the momentum of  $c(\bar{c})$ ,  $\bar{\mathbf{k}} = (\mathbf{k} - \mathbf{k}')/2$ ,  $J_V m_V$  is the total angular momentum of  $J/\Psi$ ,  $m_{s_c}$  and  $m_{s_{\bar{c}}}$  are the spins of  $c$  and  $\bar{c}$ , respectively.

With the Hamiltonian Eq. (6) and neglecting the quark-quark scattering, the scattering amplitude  $T(E)$  for  $\gamma N \rightarrow VN$  process is defined by the following Lippmann-Schwinger equation,

$$T(E) = H' + T(E) \frac{1}{E - H_0 + i\epsilon} H'. \quad (10)$$

where

$$H' = \Gamma_{\gamma,c\bar{c}} + v_{cN}. \quad (11)$$

Inserting the intermediate states of  $|VN\rangle, |c\bar{c}N\rangle$  and keeping only the first order in electromagnetic coupling  $e$  in Eq. (10), we obtain

$$T_{VN,\gamma N}^D(E) = B_{VN,\gamma N}(E) + T_{VN,\gamma N}^{(\text{fsi})}(E), \quad (12)$$

where  $B_{VN,\gamma N}(E)$  is the Born term of  $J/\psi$  photoproduction and the FSI term  $T_{VN,\gamma N}^{(\text{fsi})}(E)$  is required by the unitary condition and is defined by

$$T_{VN,\gamma N}^{(\text{fsi})}(E) = T_{VN,VN}(E) \frac{1}{E - H_0 + i\epsilon} B_{VN,\gamma N}. \quad (13)$$

In this work, we assume that the  $VN$  potential can be constructed by the Folding model using the quark- $N$  interaction  $v_{cN}$  and the wavefunction  $\phi_V$  generated from Eq. (8)

$$V_{VN,VN} = \langle \phi_V, N | \sum_c v_{cN} | \phi_V, N \rangle. \quad (14)$$

The wavefunction and  $v_{cN}$  potential are also used to construct the  $J/\Psi$  photo-production process with the following form

$$B_{VN,\gamma N} = \langle \phi_V, N | \left[ \sum_c v_{cN} \frac{|c\bar{c}\rangle \langle c\bar{c}|}{E_{c\bar{c}} - H_0} \Gamma_{\gamma,c\bar{c}} \right] | \gamma, N \rangle, \quad (15)$$

where  $E_{c\bar{c}}$  is the energy available to the propagation of  $c\bar{c}$ .

In the following, we give explicit expressions of the matrix elements of  $V_{VN,VN}$ ,  $B_{VN,\gamma N}$ , and  $T_{VN,\gamma N}^{(\text{fsi})}$ .

### 1. Matrix elements of $V_{VN,VN}$

To evaluate Eq. (14), we assume for simplicity that quark- $N$  interaction,  $v_{cN}$ , is independent of spin variables,

$$\begin{aligned} \langle \mathbf{k} m_{s_c}, \mathbf{p} m_{s_N} | v_{cN} | \mathbf{k}' m'_{s_c}, \mathbf{p}' m'_{s_N} \rangle \\ = \delta_{m_{s_c}, m'_{s_c}} \delta_{m_{s_N}, m'_{s_N}} \delta(\mathbf{k} + \mathbf{p} - \mathbf{k}' - \mathbf{p}') \langle \mathbf{q} | v_{cN} | \mathbf{q}' \rangle, \end{aligned} \quad (16)$$

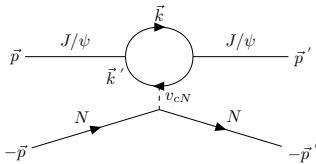


FIG. 4:  $J/\Psi$ - $N$  scattering indicate to Eq. (20) with  $v_{cN}$  potential as quark- $N$  interaction in the scattering.

where the relative momenta of quark and nucleon are defined by

$$\mathbf{q} = \frac{m_N \mathbf{k} - m_c \mathbf{p}}{m_N + m_c}, \quad (17)$$

$$\mathbf{q}' = \frac{m_N \mathbf{k}' - m_c \mathbf{p}'}{m_N + m_c}. \quad (18)$$

Here  $m_c$  and  $m_N$  are the masses of the quark  $c$  and the nucleon, respectively.

With the  $J/\Psi$  wavefunction given in Eq. (9) and the spin independent quark- $N$  potential defined by Eq. (16), we define the matrix element of the potential  $V_{VN,VN}$  given by Eq. (14) in the CM frame, where  $\mathbf{p}_V = -\mathbf{p}$  and  $\mathbf{p}'_V = -\mathbf{p}'$  as illustrated in Fig. 4. In this frame, the matrix element of Eq. (14) can be written as

$$\begin{aligned} \langle \mathbf{p}_V m_V, \mathbf{p} m_s | V_{VN,VN} | \mathbf{p}'_V m'_V, \mathbf{p}' m'_s \rangle \\ = \delta_{m_V, m'_V} \delta_{m_s, m'_s} \delta(\mathbf{p}_V + \mathbf{p} - \mathbf{p}'_V - \mathbf{p}') \langle \mathbf{p} | V_{VN} | \mathbf{p}' \rangle, \end{aligned} \quad (19)$$

where

$$\begin{aligned} \langle \mathbf{p} | V_{VN} | \mathbf{p}' \rangle &= 2 \int d\mathbf{k} \phi^*(\mathbf{k} - \frac{\mathbf{p}}{2}) \\ &\times \left\langle \mathbf{p} - \frac{m_N}{m_N + m_c} \mathbf{k} \left| v_{cN} \right| \mathbf{p}' - \frac{m_N}{m_N + m_c} \mathbf{k} \right\rangle \\ &\times \phi\left(\mathbf{k} - \frac{\mathbf{p}'}{2}\right). \end{aligned} \quad (20)$$

Here the factor 2 arises from summation of contributions from the two quarks within the  $J/\psi$  meson and we have used the definitions of Eqs. (17) and (18).

For a potential  $v_{cN}(r)$  depending only on the relative distance  $r$  between  $c$  and  $N$ , we have

$$\begin{aligned} \langle \mathbf{q} | v_{cN} | \mathbf{q}' \rangle &= v_{cN}(\mathbf{q} - \mathbf{q}') \\ &= \frac{1}{(2\pi)^3} \int d\mathbf{r} e^{i(\mathbf{q}-\mathbf{q}')\cdot\mathbf{r}} v_{cN}(r). \end{aligned} \quad (21)$$

The matrix element of  $v_{cN}$  in Eq. (20) can then be written as

$$\left\langle \mathbf{p} - \frac{m_N}{m_N + m_c} \mathbf{k} \left| v_{cN} \right| \mathbf{p}' - \frac{m_N}{m_N + m_c} \mathbf{k} \right\rangle = v_{cN}(\mathbf{p} - \mathbf{p}'). \quad (22)$$

For later calculations, we note here that for a Yukawa form  $v_{cN} = \alpha \frac{e^{-\mu r}}{r}$ , Eq. (21) leads to

$$v_{cN}(\mathbf{p} - \mathbf{p}') = \alpha \frac{1}{(2\pi)^2} \frac{1}{(\mathbf{p} - \mathbf{p}')^2 + \mu^2}. \quad (23)$$

Using Eq. (22), Eq. (20) can now be expressed in the following factorized form:

$$\langle \mathbf{p} | V_{VN} | \mathbf{p}' \rangle = F_V(\mathbf{t}) [2v_{cN}(\mathbf{t})], \quad (24)$$

where  $\mathbf{t} = \mathbf{p} - \mathbf{p}'$ , and

$$\begin{aligned} F_V(\mathbf{t}) &= \int d\mathbf{k} \phi^* \left( \mathbf{k} - \frac{\mathbf{p}}{2} \right) \phi \left( \mathbf{k} - \frac{\mathbf{p}'}{2} \right) \\ &= \int d\mathbf{k} \phi^* \left( \mathbf{k} - \frac{\mathbf{t}}{2} \right) \phi(\mathbf{k}) \end{aligned} \quad (25)$$

is the form factor of the vector meson  $V$  and  $\phi(\mathbf{k})$  is the wavefunction of  $J/\Psi$  in momentum space.

### 2. Matrix element of $B_{VN,\gamma N}$

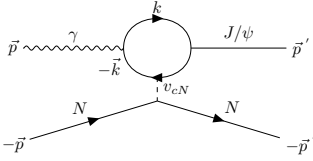


FIG. 5:  $J/\Psi$  photo-production on the proton target with the momentum variable indicate to Eq. (29).

By using the  $J/\Psi$  wavefunction and Eq. (16) for quark-N potential, the matrix element of photo-production of Eq. (15) can be calculated. With the variables in the CM system, as illustrated in Fig. 5, we obtain

$$\begin{aligned} &\langle \mathbf{p}' m_V m'_s | B_{VN,\gamma N} | \mathbf{q} \lambda m_s \rangle \\ &= \sum_{m_c, m_{\bar{c}}} \frac{1}{(2\pi)^3} \frac{e_c}{\sqrt{2|\mathbf{q}|}} \int d\mathbf{k} \langle J_V m_V | \frac{1}{2} \frac{1}{2} m_c m_{\bar{c}} \rangle \phi \left( \mathbf{k} - \frac{1}{2} \mathbf{p}' \right) \\ &\quad \times \delta_{m_s, m'_s} \left\langle \mathbf{p}' - \frac{m_N}{m_N + m_c} \mathbf{k} \left| v_{cN} \right| \mathbf{q} - \frac{m_N}{m_N + m_c} \mathbf{k} \right\rangle \\ &\quad \times \frac{1}{W - E_N(\mathbf{q}) - E_c(\mathbf{q} - \mathbf{k}) - E_c(\mathbf{k}) + i\epsilon} \\ &\quad \times \bar{u}_{m_c}(\mathbf{k}) [\epsilon_\lambda \cdot \boldsymbol{\gamma}] v_{m_{\bar{c}}}(\mathbf{q} - \mathbf{k}). \end{aligned} \quad (26)$$

If one chooses the same Yukawa form of  $v_{cN}(r)$ , one obtains the following factorized form:

$$\begin{aligned} &\langle \mathbf{p}' m_V m'_s | B_{VN,\gamma N} | \mathbf{q} \lambda m_s \rangle \\ &= C_{\lambda, m_V} \delta_{m_s, m'_s} B(\mathbf{p}', \mathbf{q}) [2v_{cN}(\mathbf{q} - \mathbf{p}')], \end{aligned} \quad (27)$$

where

$$C_{\lambda, m_V} = \sum_{m_c, m_{\bar{c}}} \langle J_V m_V | \frac{1}{2} \frac{1}{2} m_c m_{\bar{c}} \rangle \langle m_{\bar{c}} | \boldsymbol{\sigma} \cdot \boldsymbol{\epsilon}_\lambda | m_c \rangle, \quad (28)$$

and

$$\begin{aligned} B(\mathbf{p}', \mathbf{q}) &= \frac{1}{(2\pi)^3} \frac{e_c}{\sqrt{2|\mathbf{q}|}} \int d\mathbf{k} \phi \left( \mathbf{k} - \frac{1}{2} \mathbf{p}' \right) \\ &\quad \times \frac{1}{W - E_N(\mathbf{q}) - E_c(\mathbf{q} - \mathbf{k}) - E_c(\mathbf{k}) + i\epsilon} \\ &\quad \times \sqrt{\frac{E_c(\mathbf{k}) + m_c}{2E_c(\mathbf{k})}} \sqrt{\frac{E_c(\mathbf{q} - \mathbf{k}) + m_c}{2E_c(\mathbf{q} - \mathbf{k})}} \\ &\quad \times \left( 1 - \frac{\mathbf{k} \cdot (\mathbf{q} - \mathbf{k})}{[E_c(\mathbf{k}) + m_c][E_c(\mathbf{q} - \mathbf{k}) + m_c]} \right). \end{aligned} \quad (29)$$

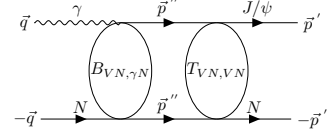


FIG. 6:  $J/\Psi$  photo-production on the proton target with final state interaction indicate to Eq. (30).

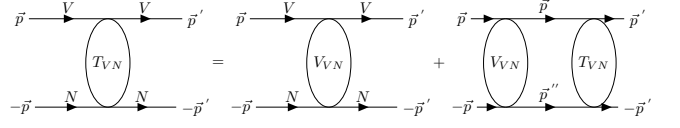


FIG. 7: The VN scattering indicate to Eq. (33).

### 3. Final State Interactions

Including the final state interaction, as illustrated in Fig. 6, the matrix element of the total amplitude in Eq. (12) is

$$\begin{aligned} \langle \mathbf{p}' m_V m'_s | T_{VN,\gamma N} | \mathbf{q} \lambda m_s \rangle &= \langle \mathbf{p}' m_V m'_s | B_{VN,\gamma N} | \mathbf{q} \lambda m_s \rangle \\ &\quad + \langle \mathbf{p}' m_V m'_s | T_{VN,\gamma N}^{(\text{fsi})} | \mathbf{q} \lambda m_s \rangle, \end{aligned} \quad (30)$$

with

$$\begin{aligned} &\langle \mathbf{p}' m_V m'_s | T_{VN,\gamma N}^{(\text{fsi})} | \mathbf{q} \lambda m_s \rangle \\ &= \sum_{m''_V, m''_s} \int d\mathbf{p}'' \langle \mathbf{p} m_V m'_s | T_{VN,VN} | \mathbf{p}'' m''_V, m''_s \rangle \\ &\quad \times \frac{1}{W - E_N(p'') - E_V(p'') + i\epsilon} \\ &\quad \times \langle \mathbf{p}'' m''_V m''_s | B_{VN,\gamma N} | \mathbf{q} \lambda, m_s \rangle. \end{aligned} \quad (31)$$

In the above equation, the spin independent amplitude of  $J/\Psi$ -N scattering is

$$\begin{aligned} &\langle \mathbf{p} m_V m_s | T_{VN,VN}(W) | \mathbf{p}' m'_V m'_s \rangle \\ &= \delta_{m_V, m'_V} \delta_{m_s, m'_s} \langle \mathbf{p}' | T_{VN}(W) | \mathbf{p} \rangle, \end{aligned} \quad (32)$$

where  $\langle \mathbf{p}' | T_{VN}(W) | \mathbf{p} \rangle$  is defined by the following Lippmann-Schwinger Equation, as illustrated in Fig. 7:

$$\begin{aligned} \langle \mathbf{p}' | T_{VN}(W) | \mathbf{p} \rangle &= \langle \mathbf{p}' | V_{VN} | \mathbf{p} \rangle \\ &\quad + \int d\mathbf{p}'' \frac{\langle \mathbf{p}' | V_{VN} | \mathbf{p}'' \rangle \langle \mathbf{p}'' | T_{VN}(W) | \mathbf{p} \rangle}{W - E_N(p'') - E_V(p'') + i\epsilon}. \end{aligned} \quad (33)$$

Here  $\langle \mathbf{p}' | V_{VN} | \mathbf{p} \rangle$  has been defined by Eq. (24).

We solve Eq. (33) in the partial-wave representation. For a spin independent  $c$ -N potential  $v_{cN}(r)$ , which gives also an spin-independent  $V_{VN}$ , we have

$$\langle \mathbf{p}' | V_{VN}(W) | \mathbf{p} \rangle = \sum_L \frac{2L+1}{4\pi} V_L(p', p, W) P_L(x), \quad (34)$$

and

$$\langle \mathbf{p}' | T_{VN}(W) | \mathbf{p} \rangle = \sum_L \frac{2L+1}{4\pi} T_L(p', p, W) P_L(x), \quad (35)$$

where  $x = \hat{\mathbf{p}} \cdot \hat{\mathbf{p}}'$  and  $P_L(x)$  is the Legendre function of the first kind. With Eq. (34), the partial-wave matrix element of potential can be calculated by

$$V_L(p', p, W) = (2\pi) \int_{-1}^{+1} dx P_L(x) \langle \mathbf{p}' | V_{VN}(W) | \mathbf{p} \rangle, \quad (36)$$

where  $\langle \mathbf{p}' | V_{VN}(W) | \mathbf{p} \rangle$  is defined by Eq. (24). If we set  $F(\mathbf{t}) = 1$  in Eq. (24) and use Eq. (23) for a Yukawa form for  $c$ - $N$  potential  $v_{cN}(r) = \alpha \frac{e^{-\mu r}}{r}$ , one finds

$$V_L(p', p, W) = \frac{2}{\pi} \left( \frac{\alpha}{2pp'} \right) Q_L(Z), \quad (37)$$

where  $Z = \frac{p^2 + p'^2 + \mu^2}{2pp'}$  and  $Q_L(Z)$  is the Legendre function of the second kind.

By using Eqs. (34)-(35), Eq. (33) then leads to

$$\begin{aligned} T_L(p', p, W) &= V_L(p', p, W) \\ &+ \int dp'' p''^2 \left[ V_L(p', p'', W) \right. \\ &\quad \times \frac{1}{W - E_N(p'') + E_V(p'') + i\epsilon} \\ &\quad \left. \times T_L(p'', p, W) \right]. \end{aligned} \quad (38)$$

We solve Eq. (38) by using the standard numerical method described in Ref. [48]. The scattering phase shifts  $\delta_L$  are calculated from the resulting  $T_L(p'', p, W)$

$$e^{i\delta_L} \sin \delta_L = -\pi \frac{p_0 E_N(p_0) E_V(p_0)}{E_N(p_0) + E_V(p_0)} T_L(p_0, p_0, W), \quad (39)$$

where the on-shell momentum defined by

$$W = E_N(p_0) + E_V(p_0). \quad (40)$$

We will also calculate the scattering length  $a$  which is defined by  $L = 0$  partial-wave at  $p_0 \rightarrow 0$  by

$$p_0 \cot \delta_0 = \frac{-1}{a}. \quad (41)$$

## B. Pomeron-exchange amplitude

Following the approach of Donnachie and Landshoff in Refs. [23, 49–51],  $T^{\text{Pom}}$  was constructed within Regge Phenomenology and is given by

$$\begin{aligned} &\langle \mathbf{k}, m_V m'_s | T_{VN, \gamma N}^{\text{Pom}}(W) | \mathbf{q}, \lambda_\gamma m_s \rangle \\ &= \frac{1}{(2\pi)^3} \sqrt{\frac{m_N m_N}{4E_V(\mathbf{k}) E_N(\mathbf{p}') |\mathbf{q}| E_N(\mathbf{p})}} \\ &\quad \times [\bar{u}(p', m'_s) \epsilon_\mu^*(k, \lambda_V) \mathcal{M}_\mathbb{P}^{\mu\nu}(k, p', q, p) \epsilon_\nu(q, \lambda_\gamma) u(p, m_s)]. \end{aligned} \quad (42)$$

In this approach, the incoming photon will be converted to vector meson, then will be scattered from nucleon by Pomeron exchange, as illustrated by Feynman diagram in Fig. 8.

The Pomeron-exchange amplitude  $\mathcal{M}_\mathbb{P}^{\mu\nu}(k, p', q, p)$  is given by

$$\mathcal{M}_\mathbb{P}^{\mu\nu}(k, p', q, p) = G_\mathbb{P}(s, t) \mathcal{T}_\mathbb{P}^{\mu\nu}(k, p', q, p), \quad (43)$$

and

$$\begin{aligned} \mathcal{T}_\mathbb{P}^{\mu\nu}(k, p', q, p) &= i 2 \frac{e m_V^2}{f_V} [2\beta_{qV} F_V(t)] [3\beta_{u/d} F_1(t)] \\ &\quad \{ \not{q} g^{\mu\nu} - q^\mu \gamma^\nu \}, \end{aligned} \quad (44)$$

where  $m_V$  is the mass of the vector meson, and  $f_V = 5.3, 15.2, 13.4, 11.2, 40.53$  for  $V = \rho, \omega, \phi, J/\Psi, \Upsilon$  are traditionally determined by calculating the  $V \rightarrow \gamma \rightarrow e^+e^-$  decay width. The parameters  $\beta_{qV}$  ( $\beta_{u/d}$ ) define the coupling of the Pomeron with the quark  $q_V$  ( $u$  or  $d$ ) in the vector meson  $V$  (nucleon  $N$ ). In Eq. (44), a form factor for the Pomeron-vector meson vertex is also introduced with

$$F_V(t) = \frac{1}{m_V^2 - t} \left( \frac{2\mu_0^2}{2\mu_0^2 + m_V^2 - t} \right), \quad (45)$$

where  $t = (q - k)^2 = (p_f - p_i)^2$ . By using the Pomeron-photon analogy, the form factor for the Pomeron-nucleon vertex is defined by the isoscalar electromagnetic form factor of the nucleon as

$$F_1(t) = \frac{4m_N^2 - 2.8t}{(4m_N^2 - t)(1 - t/0.71)^2}. \quad (46)$$

Here  $t$  is in the unit of  $\text{GeV}^2$ , and  $m_N$  is the proton mass.

The propagator  $G_\mathbb{P}$  of the Pomeron in Eq. (43) follows the Regge phenomenology form:

$$G_\mathbb{P} = \left( \frac{s}{s_0} \right)^{\alpha_P(t)-1} \exp \left\{ -\frac{i\pi}{2} [\alpha_P(t) - 1] \right\}, \quad (47)$$

where  $s = (q + p_i)^2 = W^2$ ,  $\alpha_P(t) = \alpha_0 + \alpha'_P t$ , and  $s_0 = 1/\alpha'_P$ . We use the value of  $s_0 = 0.25 \text{ GeV}$  from the works [23, 49–51] of Donnachie and Landshoff.

$T^{\text{Pom}}$  has been determined in Ref. [1, 52, 53] by fitting the data of total cross sections up to 300 GeV. The resulting parameters for  $\rho^0, \omega, \phi$  photo-production [54] have

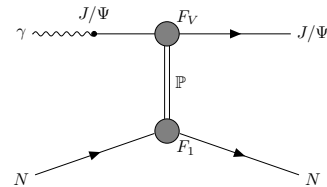


FIG. 8: The Feynman diagram of  $J/\Psi$  photoproduction with DS-pom approach

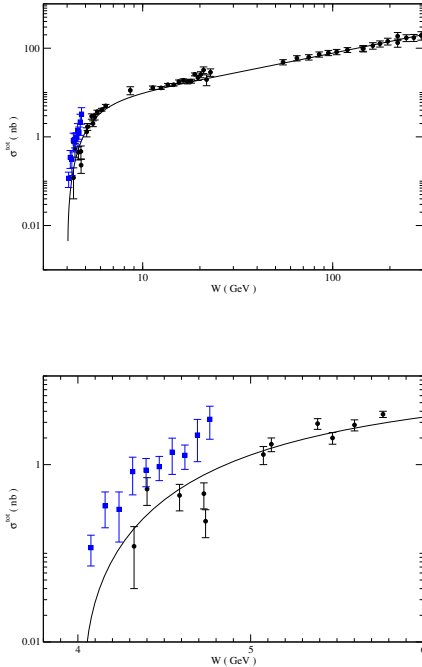


FIG. 9: Total cross sections from Pomeron-exchange amplitude for  $4 \leq W \leq 300$  GeV (top) and for  $4 \leq W \leq 6$  GeV (bottom).

been determined as follows:  $\mu_0 = 1.1$  GeV<sup>2</sup>,  $\beta_{u/d} = 2.07$  GeV<sup>-1</sup>,  $\beta_s = 1.38$  GeV<sup>-1</sup>,  $\alpha_0 = 1.08$  for  $\rho$  and  $\omega$ ,  $\alpha_0 = 1.12$  for  $\phi$ . For the heavy quark systems, we find that using the same  $\mu_0^2$ ,  $\beta_{u/d}$ , and  $\alpha'_P$  values, the photo-production data for  $J/\Psi$  and  $\Upsilon$  can be fitted by setting  $\beta_c = 0.32$  GeV<sup>-1</sup> and  $\beta_b = 0.45$  GeV<sup>-1</sup>, along with a larger  $\alpha_0 = 1.25$ .

Figure 9 depicts the total cross section for the  $J/\psi$  photo-production on the nucleon obtained solely from the contribution of the Pomeron-exchange amplitude, and compares it with the data [21, 28, 29]. One can see from Fig. 9 that while the Pomeron-exchange mechanism effectively describes the data (black circles) [28, 29] at very high energies, it falls short in accurately representing the JLab data (blue squares) [21].

### III. RESULTS

#### A. Determination of quark-Nucleon potential $v_{cN}$

We are guided by the Yukawa form of  $J/\Psi$ -N potential extracted from the LQCD calculation of Ref. [18]. We observe that the factorized form of  $V_{VN, VN}$  of Eq. (24) suggests that if  $v_{cN}(r)$  is also of the Yukawa form, the resulting  $V_{VN, VN}$  can approach the  $J/\Psi$ -N potential of Ref. [18] at large distance  $r$ . We therefore consider the

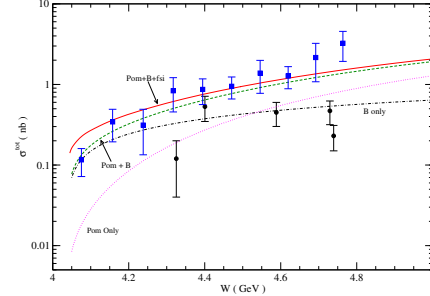


FIG. 10: Total cross sections for  $4 \leq W \leq 5$  GeV from 1Y model with  $\alpha = -0.067$ .

following parameterization

$$v_{cN}(r) = \alpha \left( \frac{-\mu r}{r} - c_s \frac{e^{-\mu_1 r}}{r} \right). \quad (48)$$

We first consider a model (1Y) with  $c_s = 0$ , meaning that the resulting  $J/\Psi$ -N potential takes on the Yukawa form extracted from LQCD. The calculation then only has two free parameters  $\alpha$  and  $\mu$ . We find that the JLab data [21] for small  $W$  region can be best fitted by choosing  $\alpha = -0.067$  and  $\mu = 0.3$  GeV if the  $J/\Psi$  wavefunction is taken from the CQM model of Ref. [43].

We show in Fig. 10 the total cross sections for the  $J/\psi$  photo-production in the small  $4 \leq W \leq 5$  GeV region obtained from the 1Y model. The dotted, dot-dashed, and dashed lines represent the results obtained from the Pomeron-exchange, Born term, and the sum of Pomeron-exchange and Born term contributions, respectively. The solid line represents the full result including the final state interaction in addition to the Pomeron-exchange and Born terms. As seen in Fig. 10, the Pomeron-exchange mechanism alone is insufficient, particularly for low-energy regimes. However, the contribution from the  $c$ -N interaction  $v_{cN}$  is essential for fitting the data in this 1Y model. In particular, the cross sections in the very near threshold region are largely determined by the FSI term. These results demonstrate that  $J/\Psi$ -N interactions can be extracted rather clearly from the  $J/\Psi$  photo-production data within this model which does not use the VMD assumption. More importantly, the calculations properly account for off-shell effects and satisfy the unitarity condition, a feature that is not considered in most, if not all, previous approaches discussed in Ref. [1].

To see the importance of using a realistic  $J/\Psi$  wavefunction, we compare the cross section from the full calculation and that from using a wavefunction that employs a momentum cut-off in evaluating  $B_{VN, \gamma N}$  amplitude. Specifically, we replace the integral  $B = \int_0^\infty \phi(k)(\dots)dk$  with  $\int_0^{k_{\max}} \phi(k)(\dots)dk$  to evaluate the cut-off effect.

In the top panel of Fig. 11, we illustrate the impact of the momentum cut-off  $k_{\max}$  on the total cross section. The solid line represents the result obtained without the

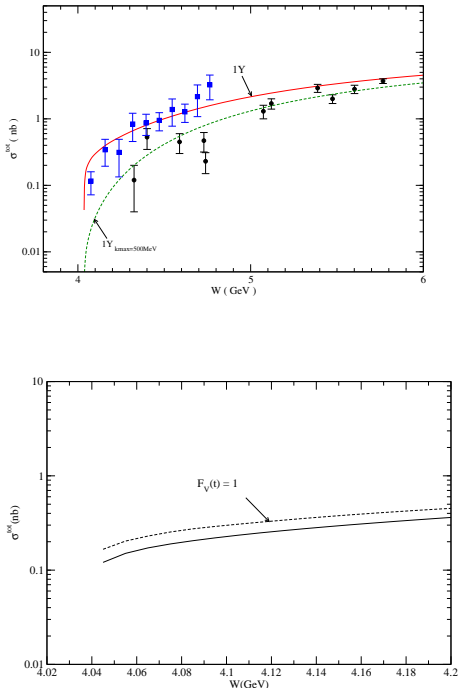


FIG. 11: The effect of the momentum cut-off  $k_{\max} = 500$  MeV (top), and the effect of the form factor (bottom), on the total cross section.

cut-off (i.e.  $k_{\max} \rightarrow \infty$ ), while the dashed line corresponds to the result obtained with the cut-off value of  $k_{\max} = 500$  MeV. Clearly, the high momentum tail of the  $J/\psi$  wavefunction is crucial for fitting the data, particularly in the low-energy region. We also note that using the Gaussian wavefunction determined by  $J/\Psi \rightarrow e^+e^-$  of Ref. [1] results in much larger cross sections, and fitting to the JLab data requires a much smaller value of  $\alpha$ .

As one can see from Eq. (24), the  $J/\Psi$ -N potential is determined by the form factor  $F_V(t)$ , which is obtained from the convolution of the initial and final state  $J/\Psi$  wavefunctions. In the bottom panel of Fig. 11, we illustrate the impact of  $F_V(t)$  on the total cross section by comparing the momentum-dependent form factor  $F_V(t)$  (solid line) with the constant form factor  $F_V(t) = 1$  (dashed line). It is evident that the effect of  $F_V(t)$  on the total cross section is significant, underscoring the importance of using a realistic  $J/\Psi$  wavefunction in determining the FSI effects.

### B. The 2Y model

We now consider the model (2Y) by incorporating the second term with  $c_s = 1$  in addition to the first term in Eq. (48). The cut-off of the short-range part is set as

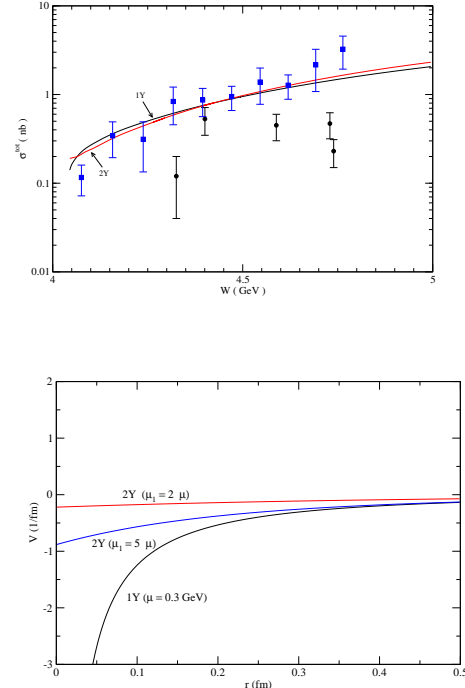


FIG. 12: (Top) Total cross sections from 1Y model with  $\alpha = -0.067$  and 2Y model with  $\alpha = -0.145$  and  $N = 5$ . (Bottom) Short-range behavior of  $v_{cN}(r)$  for the 1Y and 2Y models.

$\mu_1 = N\mu$ . We observe that for large values of  $N > 50$ , the 2Y model closely approximates the 1Y model, and the JLab data can be fitted with any  $N < 20$  by adjusting the coupling constant  $\alpha$ . The result of the total cross section from the 2Y model with  $N = 5$  and  $\alpha = -0.145$  is comparable to that of 1Y model with  $\alpha = -0.067$ , as shown in the top panel of Fig. 12. The two models fit the JLab data equally well, but have very large difference at very near threshold which is dominated completely by FSI. The origin of it is that they have very different short range behaviors of the potentials  $v_{cN}(r)$ , as shown in the bottom panel of Fig. 12. To compare the potential for 1Y model (black line), we evaluate for the 2Y model with  $N = 2$  (red line) and  $N = 5$  (blue line), using the same  $\alpha = -0.145$  for both  $N$  values. This ensures clear comparisons of their  $r$ -dependence at short distances.

We thus expect that their difference in differential cross section must be large at large  $t$ . This is shown in Fig. 13 where the differential cross sections as a function of  $t$  from the 1Y model with  $\alpha = -0.067$  and the 2Y model with  $\alpha = -0.145$  and  $N = 5$  are compared. Both models describe reasonably well the JLab data from the GlueX Collaboration [22] at  $E_\gamma = 8.8 - 10.53$  GeV. We observed that notable differences between the predictions of the 1Y and 2Y models at large values of  $t$ . More precise data are clearly needed for making further progress, while 2Y

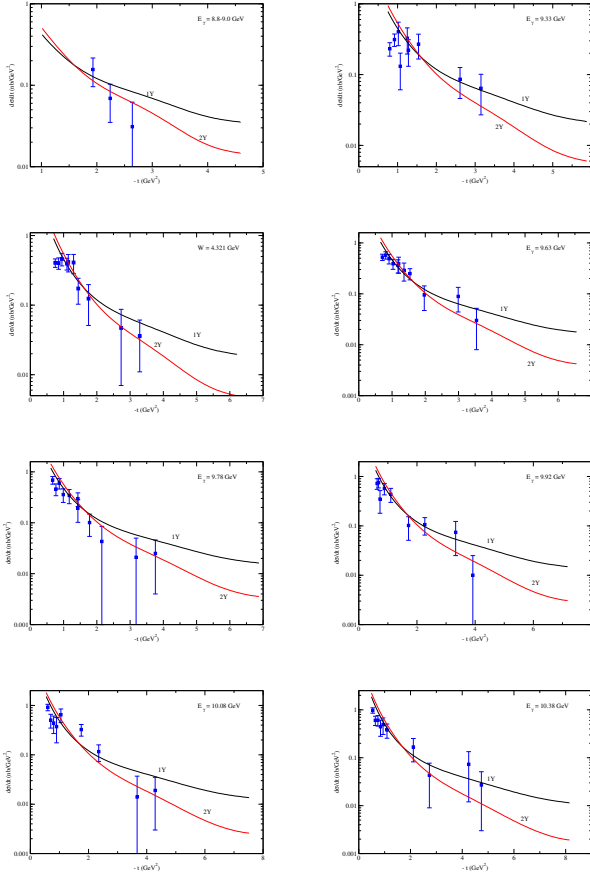


FIG. 13: Differential cross sections from 1Y model with  $\alpha = -0.067$  and 2Y model with  $\alpha = -0.145$  and  $N = 5$ .

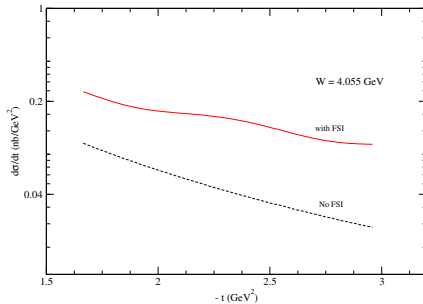


FIG. 14: Prediction of the differential cross sections near threshold at  $W = 4.055$  GeV by using 2Y model.

model appears to be better. For future experiment at very near threshold, we present in Fig. 14 the differential cross sections at  $W = 4.055$  GeV. We compare the predictions of the 2Y model with (solid line) and without (dashed line) including FSI.

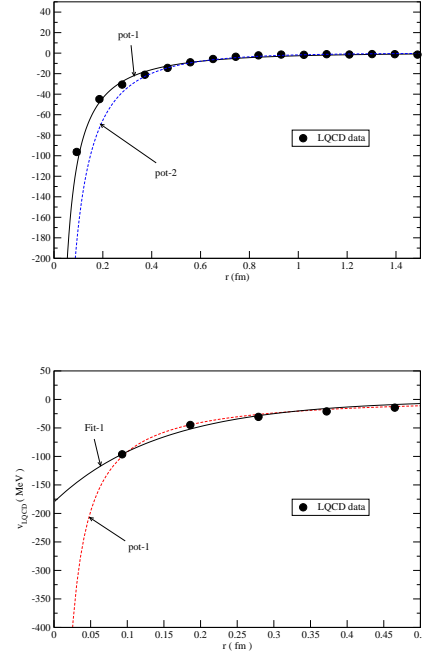


FIG. 15: The  $J/\Psi$ -N potential  $V_{J/\Psi N, J/\Psi N}(r) = \alpha_L \frac{e^{-\mu_L r}}{r}$  extracted from the LQCD calculations [18, 55].

### C. LQCD constraints

We have found that the  $J/\Psi$ -N potentials resulted from fitting the JLab data in the previous section give  $J/\Psi$ -N scattering lengths,  $-a \sim 0.3 - 0.7$  fm, which are rather different from those extracted from the LQCD of Ref. [18], as discussed in section I. Thus it raises the question on our parameterization of quark-N potential  $v_{cN}(r)$ . At low energies, the  $J/\Psi$ -N system has a small relative momentum and the multi-gluon exchange involving two quarks in  $J/\Psi$  may play important roles, and we need to extend our parameterization of  $v_{cN}$  to include two-body operator. We, however, will not explore this possibility in this exploratory work because the model will then have too many parameters which can not be determined by the still very limited data in the near threshold region. Instead, we next consider the models imposing LQCD constraints on FSI and just use their LQCD data of  $V_{J/\Psi N}(r) = \alpha_L \frac{e^{-\mu_L r}}{r}$ , where  $\alpha_L = -0.06 \sim -0.11$  and  $\mu_L = 0.3 \sim 0.5$  (in unit of GeV) [18, 55] to determine the parameters of our 1Y model with  $F_V(t) = 1$ , i.e.  $V_{J/\Psi N}^{1Y}(r) = 2v_{cN}(r) = 2\alpha \frac{e^{-\mu r}}{r}$  as one can see from Eqs. (24) and (48).

We have obtained three  $V_{J/\Psi N}(r)$  which all fit LQCD data at large  $r$ , with different short-range parts, as showing Fig. 15.

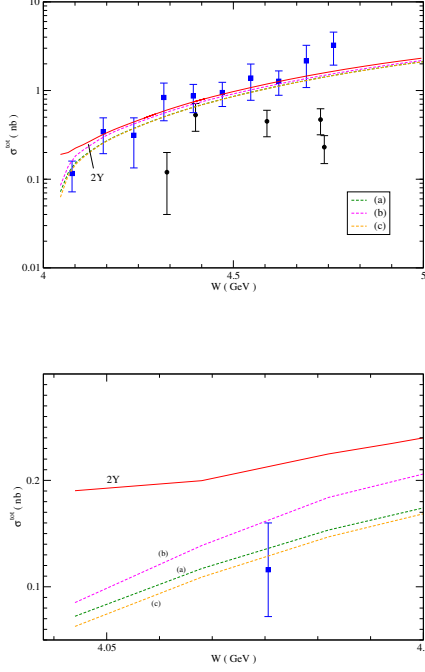


FIG. 16: Total cross-sections of  $J/\Psi$  obtained from the three models (a), (b), (c) constrained by the LQCD data with the common  $\alpha_B = -0.145$  for  $4 \leq W \leq 5$  GeV (top) and for the near threshold region (bottom).

The potential fits “pot-1” and “pot-2” are obtained from the two limiting sets for  $\alpha_L$ , i.e.  $(\alpha_L, \mu_L) = (-0.06, 0.3)$  and  $(-0.11, 0.5)$ , respectively. Since the parameter  $\alpha_L$  corresponds to  $2\alpha$  in our model, we utilize the parameter sets  $(\alpha \equiv \alpha_{\text{FSI}}, \mu) = (-0.03, 0.3)$  fixed from pot-1 and  $(-0.055, 0.5)$  fixed from pot-2. The potential labeled as “Fit-1” in Fig. 15 corresponds to the 2Y model fit to LQCD data. For this fit, we utilized the parameter set  $(\alpha_{\text{FSI}}, \mu) = (-0.1, 0.3)$  with  $N = 2$  to accurately describe the LQCD constraints on FSI. Consequently, each potential’s parameter set for the contribution of the  $T_{J/\Psi N, J/\Psi N}^{(\text{fsi})}$  term was fixed in this manner.

For the potential parameter of the Born term  $B_{J/\Psi N, \gamma N}$ , we first tried the fixed  $\alpha_B = -0.145$  obtained from the 2Y model. Combining both Born- and FSI-terms, we now construct the three models from the three potentials (pot-1, pot-2, Fit-1), i.e. model (a) with  $(\alpha_{\text{FSI}}, \alpha_B, \mu) = (-0.03, -0.145, 0.3)$  and model (b) with  $(\alpha_{\text{FSI}}, \alpha_B, \mu) = (-0.055, -0.145, 0.5)$ , and model (c) with  $(\alpha_{\text{FSI}}, \alpha_B, \mu, N) = (-0.1, -0.145, 0.3, 5)$ . We note that these three models share a common parameter  $\alpha_B$ .

Using those three models, we plot in Fig. 16 the total cross sections for  $4 \leq W \leq 5$  (GeV) region (top) and for the near threshold region (bottom), respectively. For comparison, we also plot the result obtained from the pure 2 Y model with  $(\alpha_B, \mu, N) = (-0.145, 0.3, 5)$ . As depicted in the top panel of Fig. 16, no significant dif-

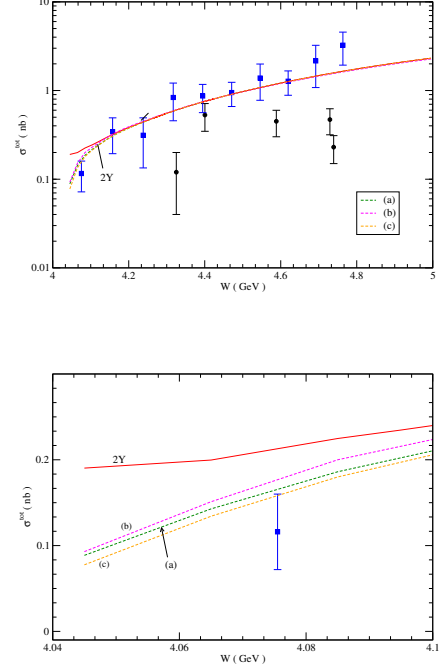


FIG. 17: Total cross-sections of  $J/\Psi$  obtained from the three models (a), (b), (c) listed in Table I for  $4 \leq W \leq 5$  GeV (top) and for the near threshold region (bottom).

ference is observed between the models imposing LQCD constraints on FSI and the pure 2Y model. However, as illustrated in the bottom panel, the models imposing LQCD constraints on FSI also exhibit a notable effect at  $W \leq 4.1$  GeV compared to the pure 2Y model. This observation indicates that the models imposing LQCD constraints on FSI improve the threshold behavior and predict the cross-section closer to the JLab data than the pure 2Y model. Additionally, we observe that it is possible to adjust the model (c) to closely match the predictions of the model (a).

To enhance our results in comparison to the JLab data [21], we attempted to adjust the parameters  $\alpha_B$  of the Born term for each model while keeping the parameters of the FSI term fixed. The best-fit parameters for each model are summarized in Table I. The scattering length  $a$  is predicted from the  $T^D$  matrix, with the other listed model parameters set accordingly.

Using the model parameters listed in Table I, we present a comparison of cross sections among the models in Fig. 17. Especially, the bottom panel of Fig. 17 displays a linear plot of the cross section at very near threshold energies ( $W \leq 4.1$  GeV). It illustrates the notable improvement achieved by the  $J/\Psi$ -N potentials extracted from LQCD calculations, especially in the region close to the threshold.

The comparison of predicted differential cross sections as a function of  $t$  is shown in Fig. 18. We compared

TABLE I: The parameters for the models (a),(b),(c) imposing LQCD constraints on FSI.

Model	$\alpha_{\text{FSI}}$	$\mu$ (GeV)	$\mu_1$ (GeV)	$a$ (fm)	$\alpha_B$
(a)	-0.03	0.3	-	-0.15	-0.162
(b)	-0.055	0.5	-	-0.233	-0.152
(c)	-0.1	0.9	1.8	-0.057	-0.163

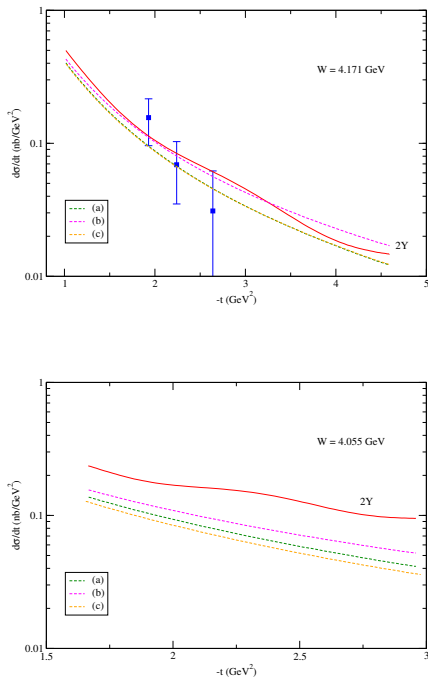


FIG. 18: Differential cross sections for each model listed in Table I.

the models' predictions at the energy closest to the JLab data [22] threshold. We observe that modifying the FSI with the LQCD potential, using a fixed parameter, yields predictions that closely match the data compared to the pure 2Y prediction. By observing the cross section and differential cross section predictions, the LQCD constraint can improve the 2Y model to have good behavior at very near threshold and at a large  $t$ .

#### D. Predictions of $\eta_c(1S)$ and $\Psi(2S)$

With the parameters of  $v_{cN}$  determined from fitting the JLab data, we proceed to predict the photo-production of  $\eta_c(1S)$  and  $\Psi(2s)$  mesons, in addition to  $J/\psi$ . Because  $v_{cN}$  is spin independent and the wavefunctions for  $\eta_c(1S)$  and  $\Psi(2S)$  are also of the  $s$ -wave form Eq. (9), the calculations can be done by using the same formula presented in section III by simply changing the wavefunctions and the kinematics associated with

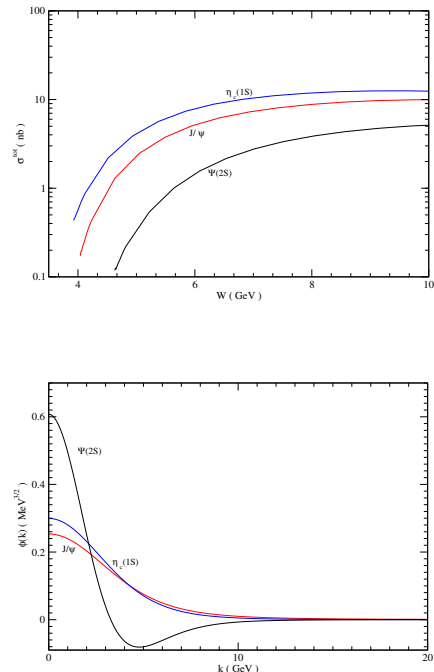


FIG. 19: The prediction of  $\eta_c(1S)$  and  $\Psi(2S)$  total cross sections (left), and the wavefunctions of  $J/\Psi$ ,  $\eta_c(1S)$  and  $\Psi(2S)$  (right).

the masses of mesons. The predicted total cross sections for the photo-productions of  $\eta_c(1S)$ ,  $\Psi(2s)$ , and  $J/\psi$  are presented in the top panel of Fig. 19, along with the comparison of their wavefunctions in the bottom panel. Using the pure 2Y model with  $(\alpha, \mu, N) = (-0.145, 0.3, 5)$ , we predicted the differential cross sections for  $\eta_c(1S)$  at 20 MeV (upper left) and 500 MeV (upper right), and for  $\Psi(2S)$  at 20 MeV (lower left) and 500 MeV (lower right) in Fig. 20.

As a validation test for our model, it would be intriguing to compare our predictions with forthcoming data expected from experiments at JLab and the future EIC.

## IV. SUMMARY AND FUTURE IMPROVEMENTS

Within a Hamiltonian formulation [24–27], a dynamical model based on the Constituent Quark Model (CQM) and a phenomenological charm quark-nucleon potential  $v_{cN}(r)$  is constructed to investigate the  $J/\Psi$  photo-production on the nucleon at energies near threshold. The main feature of the model lies in the quark-N potential,  $v_{cN}$ , which generates a photo-production amplitude defined by a  $c\bar{c}$ -loop integration over the  $\gamma \rightarrow c\bar{c}$  vertex function and the  $J/\Psi$  wavefunction,  $\Phi_{J/\Psi}(c\bar{c})$ , from the CQM described in Ref. [43]. In addition, the  $J/\Psi$ -N final state interaction is calculated from a  $J/\Psi$ -nucleon poten-

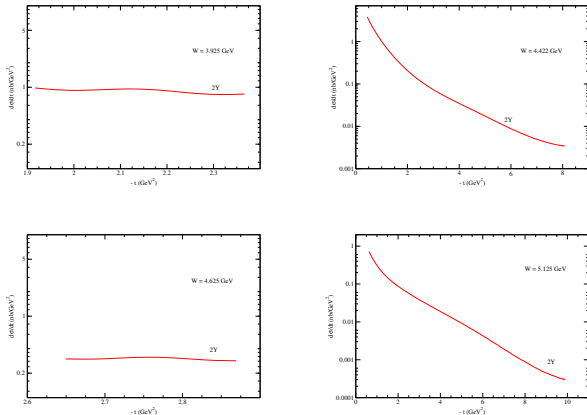


FIG. 20: (Upper) Prediction of  $\eta_c(1S)$  differential cross sections at 20 MeV (left) and 500MeV (right) from threshold. (Lower) Prediction of  $\Psi(2S)$  differential cross sections at 20 MeV (left) and 500MeV (right) from threshold.

tial ( $V_{J/\Psi N}(r)$ ) which is constructed by folding  $v_{cN}(r)$  into the same wavefunction  $\Phi_{J/\Psi}(c\bar{c})$ . By also incorporating the Pomeron-exchange amplitudes determined in Refs. [1, 53], the constructed model can describe the available data from threshold to high energies, up to the invariant mass  $W = 300$  GeV.

The parametrization of the  $c$ -N potential  $v_{cN}(r)$  is chosen such that the predicted  $V_{J/\Psi N}(r)$  at large distances has the same Yukawa potential form extracted from a LQCD calculation. The parameters of  $v_{cN}$  are determined by fitting the total cross section data of JLab's Hall-D by performing calculations that include  $J/\Psi$ -N final state interactions, as required by the unitarity condition. The predicted differential cross sections  $d\sigma/dt$  are in reasonably good agreements with the data from JLab's Hall-C. Furthermore, it is shown that the FSI effects dominate the cross section in the very near-threshold region. This indicates that the low energy  $J/\Psi$ -N scattering amplitudes and the associated models of  $J/\Psi$ -N potentials  $V_{J/\Psi N}(r)$  can be extracted from the  $J/\Psi$  photo-production data with high sensitivity. The determined  $V_{J/\Psi N}(r)$  can be used to understand the nucleon resonances  $N^*(P_c)$  reported by the LHCb collaboration [2–5], to extract the gluonic distributions in nuclei,  $J/\Psi$  pro-

duction in relativistic heavy-ion collisions, and to study the existence of nuclei with hidden charms [6–10].

By imposing the constraints of  $J/\Psi$ -N potential extracted from the LQCD calculation of Ref. [18], we have obtained three  $J/\Psi$ -N potentials which fit the JLab data equally well. The resulting  $J/\Psi$ -N scattering lengths are in the range of  $a = (-0.05 \text{ fm} \sim -0.25 \text{ fm})$ , which rule out the existence of free  $J/\Psi$ -N bound states. On the other hand, the available data near threshold is far from sufficient to draw a conclusion. Clearly, more extensive and precise experimental data are needed to make further progress.

With the determined  $c$ -N potential  $v_{cN}(r)$  and the wavefunctions generated from the same CQM of Ref. [43], the constructed dynamical model has been used to predict the cross sections of photo-production of  $\eta_c(1S)$  and  $\Psi(2S)$  mesons. It will be interesting to have data from experiments at JLab and EIC to test our predictions.

The model presented here needs to be improved in the future. Our parametrization of quark-nucleon potential  $v_{cN}$  is guided by the Yukawa form extracted from a LQCD calculation of Ref. [18]. This must be improved by using more advanced LQCD calculations of  $J/\Psi$ -N scattering, in particular the short-range part of the potential. A recent LQCD calculation of  $\phi$ -N interaction leads to a more complex form than the simple Yukawa form.

It is necessary to improve our model by developing  $c\bar{c}$ -loop calculations of Pomeron-exchange mechanism which is needed to fit high energy data. This requires an extension of our approach to include relativistic effects. This can be done straightforwardly within the Instant Form of relativistic Quantum Mechanics of Dirac [34], while the Light-front form is also possible with much more works.

## ACKNOWLEDGEMENT

We would like to thank J. Segovia for providing us with the CQM wavefunctions used in this work. The works of S.S and H.-M.C. were supported by the National Research Foundation of Korea (NRF) under Grant No. NRF- 2023R1A2C1004098. The work of T.-S.H.L. was supported by the U.S. Department of Energy, Office of Science, Office of Nuclear Physics, under Contract No.AC02-06CH11357.

- 
- [1] T.-S. H. Lee, S. Sakinah, Yongseok Oh, Models of  $J/\Psi$  photo-production reactions on the nucleon, *Eur. Phys. J.A* **58**, 12 252 (2023).  
 [2] R. Aaij *et al.*, LHCb Collaboration, Observation of  $J/\psi p$  resonances consistent with pentaquark states in  $\Lambda_b^0 \rightarrow J/\psi K^- p$  decays, *Phys. Rev. Lett.* **115**, 072001 (2015).  
 [3] R. Aaij *et al.*, LHCb Collaboration, Evidence for exotic hadron contributions to  $\Lambda_b^0 \rightarrow J/\psi p \pi^-$  decays, *Phys.*

- Rev. Lett.* **117**, 082003 (2016).  
 [4] R. Aaij *et al.*, Observation of a narrow pentaquark state,  $P_c(4312)^+$ , and of the two-peak structure of the  $P_c(4450)^+$ , *Phys. Rev. Lett.* **122**, 222001 (2019).  
 [5] R. Aaij *et al.*, LHCb Collaboration, Evidence for a new structure in the  $J/\psi p$  and  $J/\psi \bar{p}$  systems in  $B_s^0 \rightarrow J/\psi p \bar{p}$  decays, *Phys. Rev. Lett.* **128**, 062001 (2022).

- [6] S. J. Brodsky, G. F. de Teramond, Spin correlations, QCD color transparency, and heavy-quark thresholds in proton-proton scattering, *Phys. Rev. Lett.* **60**, 1924 (1988).
- [7] S. J. Brodsky, I. Schmidt, G. F. de Teramond, Nuclear-bound quarkonium, *Phys. Rev. Lett.* **64**, 1011 (1990).
- [8] H. Gao, T.-S. H. Lee, V. Marinov,  $\phi$ - $N$  bound state, *Phys. Rev. C* **63**, 022201(R) (2001).
- [9] V. B. Belyaev, N. V. Shevchenko, A. Fix, W. Sandhas, Binding of charmonium with two- and three-body nuclei, *Nucl. Phys. A* **780**, 100 (2006).
- [10] J.-J. Wu, T.-S. H. Lee, Photoproduction of bound states with hidden charm, *Phys. Rev. C* **86**, 065203 (2012).
- [11] M. E. Peskin, Short-distance analysis for heavy-quark systems (I). Diagrammatics, *Nucl. Phys. B* **156**, 365 (1979).
- [12] G. Bhanot, M. E. Peskin, Short-distance analysis for heavy-quark systems (II). Applications, *Nucl. Phys. B* **156**, 391 (1979).
- [13] M. Luke, A. V. Manohar, M. J. Savage, A QCD calculation of the interaction of quarkonium with nuclei, *Phys. Lett. B* **288**, 355 (1992).
- [14] S. J. Brodsky, G. A. Miller, Is  $J/\psi$ -nucleon scattering dominated by the gluonic van der Waals interaction?, *Phys. Lett. B* **412**, 125 (1997).
- [15] A. B. Kaidalov, P. E. Volkovitsky, Heavy-quark interactions with nucleons and nuclei, *Phys. Rev. Lett.* **69**, 3155 (1992).
- [16] N. Ishii, S. Aoki, T. Hatsuda, Nuclear force from lattice QCD, *Phys. Rev. Lett.* **99**, 022001 (2007).
- [17] S. Aoki, T. Hatsuda, N. Ishii, Theoretical foundation of the nuclear force in QCD and its applications to central and tensor forces in quenched lattice QCD simulations, *Prog. Theor. Phys.* **123**, 89 (2010).
- [18] T. Kawanai, S. Sasaki, Charmonium-nucleon potential from lattice QCD, *Phys. Rev. D* **82**, 091501(R) (2010).
- [19] T. Kawanai, S. Sasaki, Charmonium-nucleon interaction from lattice QCD with 2+1 flavors of dynamical quarks, *AIP Conf. Proc.* **1388**, 640 (2011).
- [20] Y.-Z. Xu, S.-Y. Chen, Z.-Q. Yao, D. Binosi, Z.-F. Cui, C. D. Roberts, Vector-meson production and vector meson dominance, *Eur. Phys. J. C* **81**, 895 (2021).
- [21] A. Ali *et al.*, GlueX Collaboration, First measurement of near-threshold  $J/\psi$  exclusive photoproduction off the proton, *Phys. Rev. Lett.* **123**, 072001 (2019).
- [22] S. Adhikari *et al.*, GlueX Collaboration, Measurement of the  $J/\psi$  photoproduction cross section over the full near-threshold kinematic region, *Phys. Rev. C* **108**, 025201 (2023).
- [23] A. Donnachie, P. V. Landshoff, Elastic scattering and diffraction dissociation, *Nucl. Phys. B* **244**, 322 (1984).
- [24] T. Sato, T.-S. H. Lee, Meson-exchange model for  $\pi N$  scattering and  $\gamma N \rightarrow \pi N$  reaction, *Phys. Rev. C* **54**, 2660 (1996).
- [25] A. Matsuyama, T. Sato, T.-S. H. Lee, Dynamical coupled-channel model of meson production reactions in the nucleon resonance region, *Phys. Rep.* **439**, 193 (2007).
- [26] B. Juliá-Díaz, T.-S. H. Lee, A. Matsuyama, T. Sato, Dynamical coupled-channels model of  $\pi N$  scattering in the  $W \leq 2$  GeV nucleon resonance region, *Phys. Rev. C* **76**, 065201 (2007).
- [27] H. Kamano, S. X. Nakamura, T.-S. H. Lee, T. Sato, Nucleon resonances within a dynamical coupled-channels model of  $\pi N$  and  $\gamma N$  reactions, *Phys. Rev. C* **88**, 035209 (2013).
- [28] M. Derrick *et al.*, ZEUS Collaboration, Measurement of the cross section for the reaction  $\gamma p \rightarrow J/\psi p$  with the ZEUS detector at HERA, *Phys. Lett. B* **350**, 120 (1995).
- [29] C. Adloff *et al.*, H1 Collaboration, Elastic photoproduction of  $J/\psi$  and  $\Upsilon$  mesons at HERA, *Phys. Lett. B* **483**, 23 (2000).
- [30] C. D. Roberts and A. G. Williams, Dyson-Schwinger equations and their application to hadronic physics, *Prog. Part. Nucl. Phys.* **33**, 477 (1994).
- [31] C. D. Roberts, Electromagnetic pion form factor and neutral pion decay width, *Nucl. Phys. A* **605**, 475 (1996).
- [32] M. A. Pichowsky, T.-S. H. Lee, Pomeron-exchange and exclusive electroproduction of  $\rho$ -mesons in QCD, *Phys. Lett. B* **379**, 1 (1996).
- [33] M. A. Pichowsky, T.-S. H. Lee, Exclusive diffractive processes and the quark substructure of mesons, *Phys. Rev. D* **56**, 1644 (1997).
- [34] B. D. Keister and W. N. Polyzou, Relativistic Hamiltonian Dynamics in Nuclear and Particle Physics, *Adv. Nucl. Phys.* **20**, 225 (1991).
- [35] P. Maris, C. D. Roberts,  $\pi$ - and  $K$ -meson Bethe-Salpeter amplitudes, *Phys. Rev. C* **56**, 3369 (1997).
- [36] L. Chang, Y.-X. Liu, C. D. Roberts, Dressed-quark anomalous magnetic moments, *Phys. Rev. Lett.* **106**, 072001 (2011).
- [37] L. Chang, I. C. Cloët, C. D. Roberts, S. M. Schmidt, P. C. Tandy, Pion electromagnetic form factor at space-like momenta, *Phys. Rev. Lett.* **111**, 141802 (2013).
- [38] S.-X. Qin, C. D. Roberts, Impressions of the continuum bound state problem in QCD, *Chinese Phys. Lett.* **37**, 121201 (2020).
- [39] Z.-Q. Yao, D. Binosi, Z.-F. Cui, C. D. Roberts, Semileptonic transitions:  $B_{(s)} \rightarrow \pi(K)$ ;  $D_s \rightarrow K$ ;  $D \rightarrow \pi, K$ ; and  $K \rightarrow \pi$ , *Phys. Lett. B* **824**, 136793 (2022).
- [40] R. Alkofer, L. von Smekal, The infrared behavior of QCD Green's functions. Confinement, dynamical symmetry breaking, and hadrons as relativistic bound states, *Phys. Rep.* **353**, 281 (2001).
- [41] H. Sanchis-Alepuz, G. Eichmann, S. Villalba-Chávez, R. Alkofer, Delta and Omega masses in a three-quark covariant Faddeev approach, *Phys. Rev. D* **84**, 096003 (2011).
- [42] G. Eichmann, C. S. Fischer, Unified description of hadron-photon and hadron-meson scattering in the Dyson-Schwinger approach, *Phys. Rev. D* **85**, 034015 (2012).
- [43] J. Segovia, D. R. Entem, F. Fernandez, E. Hernandez, Constituent quark model description of charmonium phenomenology, *Int. J. Mod. Phys. E* **22**, 1330026 (2013).
- [44] S. J. Brodsky, E. Chudakov, P. Hoyer, J. M. Laget, Photoproduction of charm near threshold, *Phys. Lett. B* **498**, 23 (2001).
- [45] Y. Guo, X. Ji, Y. Liu, QCD analysis of near-threshold photon-proton production of heavy quarkonium, *Phys. Rev. D* **103**, 096010 (2021).
- [46] K. A. Mamo, I. Zahed, Diffractive photoproduction of  $J/\psi$  and  $\Upsilon$  using holographic QCD: Gravitational form factors and GPD of gluons in the proton, *Phys. Rev. D* **101**, 086003 (2020).
- [47] Marvin L. Goldberger and Kenneth M. Watson, "Collision Theory", Robert E. Krieger Publishing Company, Huntington, New York (1975).

- [48] Michael I. Haftel and Frank Tabakin, Nuclear Saturation and the smoothness of Nucleon-Nucleon Potential., Nucl. Phys. A **158**, 1 (1970).
- [49] A. Donnachie, P. V. Landshoff, Total cross sections, Phys. Lett. B **296**, 227 (1992).
- [50] A. Donnachie, P. V. Landshoff, Exclusive vector meson production at HERA, Phys. Lett. B **348**, 213 (1995).
- [51] A. Donnachie, P. V. Landshoff, Small  $x$ : two pomerons!, Phys. Lett. B **437**, 408 (1998).
- [52] T.-S. H. Lee, Pomeron-LQCD model of  $J/\psi$  photoproduction on the nucleon, arXiv:2004.13934.
- [53] J.-J. Wu, T.-S. H. Lee, Production of  $J/\Psi$  on the nucleon and on deuteron targets, Phys. Rev. C **88**, 015205 (2013).
- [54] Y. Oh, T.-S. H. Lee, One-loop corrections to  $\omega$  photoproduction near threshold, Phys. Rev. C **66**, 045201 (2002).
- [55] S. Sasaki, private communications, (2020).